Tagtag: Material Sensing with Commodity RFID

Binbin Xie[1], Jie Xiong[1], Xiaojiang Chen[2,3], Eugene Chai[4]
Liyao Li[2,3], Zhanyong Tang[2,3], Dingyi Fang[2,3]
[1]University of Massachusetts Amherst, [2]Northwest University
[3]International Joint Research Centre for Battery-free IoT, [4]NEC Labs America

ABSTRACT

Material sensing is an essential ingredient for many IoT applications. While hyperspectral camera, infrared, X-Ray, and Radar provide potential solutions for material identification, high cost is the major concern limiting their applications. In this paper, we explore the capability of employing RF signals for fine-grained material sensing with commodity RFID device. The key reason for our system to work is that the tag antenna's impedance is changed when it is close or attached to a target. The amount of impedance change is dependent on the target's material type, thus enabling us to utilize the impedance-related *phase change* available at commodity RFID devices for material sensing. Several key challenges are addressed before we turn the idea into a functional system: (i) the random tag-reader distance causes an additional unknown phase change on top of the phase change caused by the target material; (ii) the tag rotations cause phase shifts and (iii) for conductive liquid, there exists liquid reflection which interferes with the impedance-caused phase change. We address these challenges with novel solutions. Comprehensive experiments show high identification accuracies even for very similar materials such as Pepsi and Coke.

CCS CONCEPTS

• **Computer systems organization** → *Sensors and actuators*.

KEYWORDS

Material sensing, RFID, tag, antenna impedance, conductive liquid.

ACM Reference Format:
Binbin Xie[1], Jie Xiong[1], Xiaojiang Chen[2,3], Eugene Chai[4] and Liyao Li[2,3], Zhanyong Tang[2,3], Dingyi Fang[2,3]. 2019. Tagtag: Material Sensing with Commodity RFID. In *The 17th ACM Conference on Embedded Networked Sensor Systems (SenSys '19), November 10–13, 2019, New York, NY, USA.* ACM, New York, NY, USA, 13 pages. https://doi.org/10.1145/3356250.3360027

1 INTRODUCTION

Wireless sensing has attracted considerable research attentions in recent years. Among diverse wireless technologies being employed for sensing, RFID is promising due to its wide adoption in our everyday lives. RFID technology has been widely used in asset tracking and security identification. Recent research has explored the possibilities of employing RFID for fine-grained localization and tracking [24], gesture recognition [35], vibration monitoring [48] and touch sensing [13, 31]. In this work, we would like to employ RFID for material sensing. Material sensing plays an important role in many real-life applications including context-aware interaction [5], robot control [49] and food monitoring [15, 42], etc. With material sensing, a robot can intelligently reduce its grip strength if it knows the object is an egg instead of a metal. In a smart home, material sensing can help to identify if the daily food such as milk has expired without a taste. Without opening the bottle, fine-grained material sensing can tell if an expensive bottle of perfume is genuine or not.

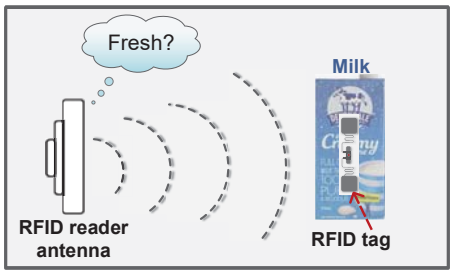

Figure 1: Material sensing by attaching passive tags.

Existing systems employ hyperspectral camera [3], infrared [33], mass spectrometry [17], high frequency X-Ray [30] and large-bandwidth Radar [49] for material sensing. These equipments are usually expensive. Furthermore, camera-based systems have difficulties to sense the target inside a non-transparent case. Recently, Wang et al. [42] and Ashutosh et al. [8] exploited RFID and UWB signals respectively for material identification. They move a big step in this direction. However, the proposed systems (TagScan & LiquID) require the signal to penetrate through the target to sense the material type and thus the targets need to be placed inside a specific zone between the transmitter and receiver for sensing. In addition, both systems can only sense one target at a time and the first target needs to be removed before the second target can be sensed.

This paper introduces Tagtag, a more flexible system that attaches RFID tags on the target for fine-grained material sensing as shown in Figure 1. Note that the tags do not need to have immediate contact with the target. We can attach the tags to the case/box/cup and sense the material inside. Not only for material identification, our system is also able to monitor the changes of the material such as milk expiration without opening the bottle. The target is not restricted to be placed in a particular zone for sensing. As long as the reader is able to communicate with the tag, the target material can be sensed so the size of the sensing area is greatly increased with just one RFID reader compared with the state-of-the-arts. Furthermore, our proposed system can sense multiple items simultaneously.

SenSys '19, November 10–13, 2019, New York, NY, USA

ACM ISBN 978-1-4503-6950-3/19/11…$15.00
https://doi.org/10.1145/3356250.3360027

Different from the existing material sensing work which employ the propagation characteristic inside the material for sensing, this work employs the property that the impedance of tag antenna gets changed when the tag is attached to a target for material sensing. We observe that the amount of impedance change is related to the target material type. Specifically, this impedance change will cause phase and RSS (receive signal strength) changes of the signal measured at the RFID reader, and these changes can be carefully processed for material sensing. Compared to RSS, the phase reading has a finer resolution [48], we thus employ the unique phase change as the *material feature* for material sensing. With the inherent channel hopping function adopted by commodity RFID, we combine material features from multiple channels to form a more stable *material pattern* for accurate sensing. Several key challenges need to be tackled before the system can work:

- **Challenge 1:** While different material types cause phase differences, varying RFID tag-reader distances also cause different phase changes. We name this issue *distance dependence* problem.
- **Challenge 2:** Random tag rotations also cause different phase changes. Requiring tags to be placed always with a same rotation is not realistic.
- **Challenge 3:** Most liquids such as water and Pepsi are conductive. These conductive liquids actually reflect a small amount of signal back and this reflected signal causes additional phase changes, interfering the phase readings and making extracting the material feature challenging.

To address Challenge 1, we propose to move the reader to a random nearby second location and with readings at two locations, we can successfully remove the tag-reader distance dependency (Section 4.2). To address Challenge 2, we discover that although random tag rotation affects the phase readings, the changes across different channels remain the same. Thus, the tag rotation only causes a same amount of change across all the channels and does not affect the envelope of the material pattern formed by multiple channels. To address Challenge 3, we discover that the reflection caused phase interference varies with the liquid thickness[1] periodically. An interesting observation is that the conductive liquid does not reflect any signal when its thickness is integer times of the signal wavelength in the liquid. By taking advantage of this observation, we can remove the reflection-caused interference to obtain reflection-free phase values for material sensing with careful signal processing.

The main contributions are summarized as follows.

- We discover the envelope of phase changes across multiple channels is unique and stable for each material. We define this unique property as *material pattern* and employ it for material sensing.
- We propose solutions to address the tag-reader distance dependency issue and tag's random rotation issue to make Tagtag more practical for real-life adoption. We further address issues including coarse RSS readings and multipath to make the system robust.
- The system is implemented on commodity off-the-shelf RFID hardware. Tagtag is able to achieve high identification accuracies even for similar liquids such as Pepsi and Coke. Tagtag is sensitive enough to detect 1g of salt in 100ml water at 100% accuracy. Tagtag can identify the fake luxury CHANEL perfume and expired milk without opening the bottle. Tagtag's sensing range is up to 3 meters. We believe this system presents a new direction in exploring the sensing capability of commodity RFID devices.

[1]Liquid thickness means the depth of liquid in the horizontal direction.

2 RELATED WORK

Wireless sensing has enabled a large range of applications including localization [7, 21, 22, 40, 46, 51, 53], tracking [18, 26, 27, 44], gesture recognition [28, 29, 50, 52], activity identification [19, 23, 36, 36] and RF-imaging [16, 20], etc. Tagtag is inspired by this trend of wireless sensing and is closely related to the work in the following domains.

RF-based material identification system. The hyperspectral camera, infrared, mass spectrometry and high frequency X-Ray are commonly used for material identification. Recently, low frequency RF technologies are being exploited as interesting alternatives for material sensing. Early RF-based material sensing work rely on 60GHz signals [49] penetrating through the targets [38, 38, 42]. On the other hand, RSA [54] captures the signals reflected from the target surface for sensing using the millimeter-wave hardware. RadarCat [49] also employs a 60GHz device to touch the target for material identification. These hardwares are relatively expensive and the millimeter-wave signals have a short propagation range, making them not cost-efficient for large-scale deployment. In contrast, Tagtag is cheaper because of the low-cost passive tags (as low as 5 cents) and each reader can work with many tags simultaneously to amortize the cost of the reader. Recently, TagScan [42] and LiquID [8] are proposed to exploit signal propagation characteristic inside the target for material identification. Both of them require the targets to be placed between the transceivers so the RF signals can penetrate through the target, limiting the size of sensing zone. The tag-reader distance also needs to be small to minimize the diffraction effect which could undermine the performance. Tagtag attaches the tags to the targets so the target has a great flexibility to be randomly placed and moved. Moreover, while the existing systems only can monitor one target at a time, Tagtag is able to sense multiple items simultaneously. Even though the RFID tag identifier can be used to label a material directly, it is not possible for the identifier to monitor the target changes such as the expiration of food inside a non-transplant container. Sarma et al. [5] attach the tags to the cups to detect the liquid volume. They employ coarse RSS readings and do not touch the liquid reflection and liquid type problem, achieving a detection rate of 81%. RFIQ [15] detects the food quality and safety by attaching one tag to the target. The liquid reflection problem is not addressed.

Tag-based sensing. Several studies have analyzed the impact of nearby targets to the RFID tag's antenna [10, 14, 32]. The methods in [14], [1] and [12] measure the change in tag antenna's gain and impedance when there is a nearby target. These systems can detect whether there is a target nearby but is not able to estimate the material type of the target. The gain and impedance changes of the RFID tag are studied with simulations in [32] when a tag is moved close to a metal plane. However, the gain and impedance values cannot be measured without dedicated hardware. Different from the previous work, Tagtag employs the fine-grained phase change which

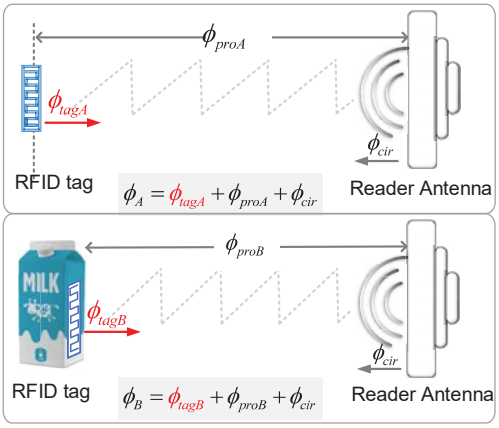

Figure 2: Phase readings before/after a tag is attached.

is available at commodity RFID reader to identify material types without a need of modifying the tag.

RFID-based sensing applications. RIO [31] detects the tag antenna impedance change brought in by the finger touch for tracking fingers. Most RFID-based systems [35, 45, 48] consider the phase change introduced by the tag antenna's impedance change as noise and they generally remove this "bad impact" using phase calibration. Tagtag exploits this phase change for material identification. Other RFID based sensing applications [4, 39] include light detection [2], humidity [25] and temperature sensing [6], etc.

3 PRELIMINARIES

When one RFID tag is attached to a target, the tag antenna's impedance gets changed. Targets of different materials cause different amounts of impedance changes. This impedance change will then cause a *phase change* at the signal backscattered from this tag, and also cause a change of power radiated from the tag [9].

3.1 Phase change caused by impedance change

In this section, we first present the general phase model [45] in RFID and show our discovery about how the material type affects the phase readings.

Phase model for an RFID system. The phase reading ϕ reported by the RFID reader contains three parts [45]

$$\phi = \phi_{tag} + \phi_{pro} + \phi_{cir}. \tag{1}$$

where ϕ_{tag} is the phase shift induced by the tag and is relevant to the tag antenna's impedance Z_a [31]. ϕ_{pro} is caused by the signal propagation of distance d in the air, and ϕ_{cir} is the phase shift introduced by the RFID reader circuit. All these three parts are unknown.

Phase change when the tag is attached to a target. As an RFID tag is attached to a target, its antenna impedance Z_a gets changed. This impedance change causes a phase change accordingly. This phase change $\Delta\phi_M$ can be defined as

$$\Delta\phi_M = \phi_{tagB} - \phi_{tagA}. \tag{2}$$

where ϕ_{tagA} and ϕ_{tagB} indicate the phase shifts caused by tag impedance before and after the tag is attached to the target. The phase change $\Delta\phi_M$ is related to target material and we define it as the *material feature*. Now let's refer to Figure 2 to illustrate the concept. Before and after the tag is attached to the target, the phase readings reported by the RFID reader are ϕ_A and ϕ_B respectively and they can be expressed as

$$\begin{cases} \phi_A = \phi_{tagA} + \phi_{proA} + \phi_{cir}. \\ \phi_B = \phi_{tagB} + \phi_{proB} + \phi_{cir}. \end{cases} \tag{3}$$

ϕ_{proA} and ϕ_{proB} represent the phase changes due to signal propagation before and after the tag is attached, and they do not need to be equal to each other. By taking the subtraction of the two equations, we obtain

$$\phi_B - \phi_A = (\phi_{tagB} - \phi_{tagA}) + \phi_{proB} - \phi_{proA}. \tag{4}$$

Further, since we defined $\Delta\phi_M = \phi_{tagB} - \phi_{tagA}$ in Eq. (2), Eq. (4) can be rewritten as

$$\phi_B = \Delta\phi_M + \phi_{proB} + \phi_A - \phi_{proA}. \tag{5}$$

ϕ_A is the phase reading measured at the RFID reader when there is no target. ϕ_{proA} is the phase change due to the signal propagation in the air when there is no target which can be calculated by measuring the distance between reader and tag. Thus both ϕ_A and ϕ_{proA} can be measured beforehand and $\phi_A - \phi_{proA}$ is a constant[2]. We define $\phi_0 = \phi_A - \phi_{proA}$. Thus, when the tag is attached to a target, the phase reading ϕ_B is only related to the material feature ($\Delta\phi_M$) and the distance-dependence phase shift (ϕ_{proB}) as below

$$\phi_B = \Delta\phi_M + \phi_{proB} + \phi_0. \tag{6}$$

3.2 RSS change caused by impedance change

When the tag is attached to a target, the tag antenna gain and its radiation coefficient get changed due to the change in radiation pattern and tag antenna impedance [9, 43]. According to the extended Friis equation [9], we can utilize Eq. (7) to quantify the reader's RSS reading with respect to the tag antenna gain G_t and its radiation coefficient Γ_{tar}

$$RSS = 10\lg(G_t^2\Gamma_{tar}\frac{P_{Tx}}{1mW}T_rG_r^2(\frac{c}{4\pi fd})^4). \tag{7}$$

where P_{Tx} is the transmission power of the reader, T_r is a constant representing the transmission loss of the RFID reader [9], d is the distance between the tag and reader antenna, and G_r is the reader antenna's gain.

Note that the phase readings of RFID system have a much finer-grained resolution (0.0015radians) compared to that of RSS readings (0.5dBm) [47]. Therefore, we employ phase change instead of RSS change as the *material feature* to identify material types and sense changes.

3.3 Impedance/Phase/RSS changes for different materials

To verify the feasibility of our idea, we conduct benchmark experiments to see how the tag antenna impedance and accordingly the phase and RSS readings change when the tag is attached to targets with different materials. To measure the tag impedance change caused by the target, we take the E41-B RFID tag's antenna[3] out

[2]This constant only needs to be measured and calculated once.

[3]Here we employ the E41-B tag to show the impedance change because it can be much more easily connected to the VNA. We employ smaller tags for all the rest experiments.

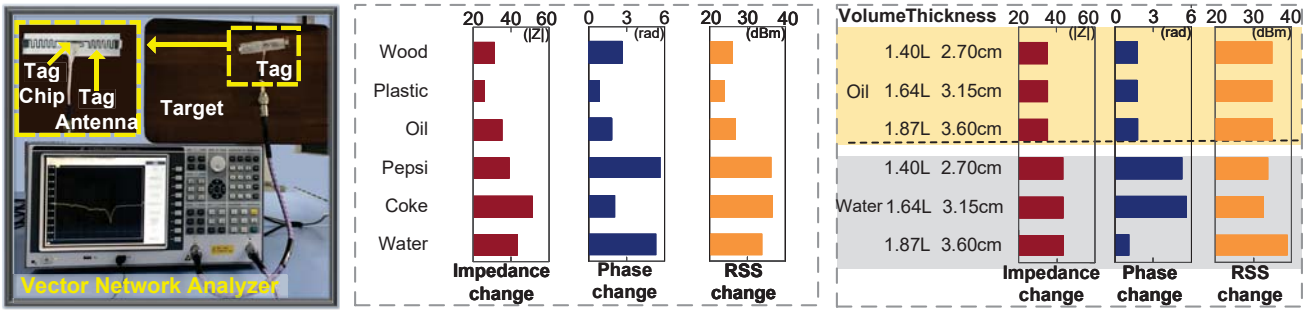

(a) VNA experiment setup. (b) Measured impedance/phase/RSS changes for different targets. (c) Analysis for conductive liquid reflection.

Figure 3: The basic idea for Tagtag's material identification.

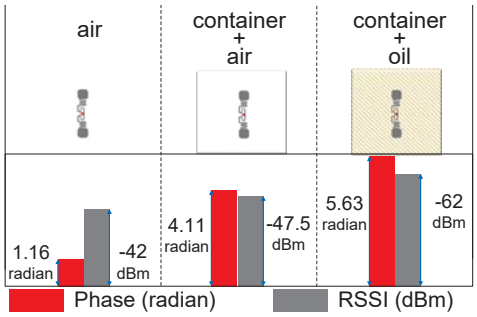

Figure 4: Both the tagged container and its internal liquid affect the tag antenna impedance.

from the chip, and solder the feed point of the tag antenna directly to the Vector Network Analyzer (VNA) equipment (AV3656A)[4] to measure the antenna's impedance value, as shown in Figure 3(a). Since the isolated antenna cannot be interrogated by the reader so we cannot obtain the RSS/phase readings, we place another E41-B tag near to the isolated E41-B tag antenna. The spacing between the second tag and the isolated antenna is kept as 15cm to make sure there is no coupling effect. This second tag 15cm away can be interrogated to obtain phase and RSS readings. Note that even though the phase/RSS readings will not be the same for two tags separated by 15cm, here we care about the phase/RSS changes and the changes for the two tags are very similar. Thus, we can measure the RSS/phase changes at the second tag (can be interrogated) to represent the changes at the first isolated tag (cannot be interrogated by the reader).

We measure the phase and RSS readings before and after the tag is attached and calculate the corresponding changes. Each type of liquid is poured into an identical rectangular-shaped container with a bottom size of $26cm \times 20cm$. The tags are attached to the bottom of the container for measurements. As shown in Figure 3(b), the impedance, phase and RSS changes for six different materials (wood, plastic, oil, Pepsi, Coke, water) are quite different. These results show that the antenna impedance does change differently when the tag is attached to different materials and accordingly both phase and RSS changes are also different.

[4]The expensive VNA helps to measure the impedance change of tag antenna while the RFID reader cannot obtain such information.

Conductive liquid reflection. Another interesting observation is that for non-conductive liquid [34] with different thicknesses (sunflower oil with thicknesses of 2.7cm, 3.15cm and 3.6cm), the impedance, phase and RSS changes are exactly the same as shown in Figure 3(c). On the other hand, for conductive liquid with different thicknesses (water with thicknesses of 2.7cm, 3.15cm and 3.6cm), the impedance changes are the same but the phase and RSS changes are dramatically different. The reason is that water of different thicknesses reflects different amounts of signals, causing different phase and RSS changes while the oil does not reflect any signal. So, when there is no reflection (e.g., oil), the same impedance change induces exactly the same amount of phase/RSS changes. However, when there is reflected signal, the overall phase change is actually composed of two parts: phase change caused by impedance change (related to target material) and phase change caused by reflection (related to target thickness). Thus, if the liquid reflects signal, the size (thickness) of the liquid also affects the phase readings, interfering the impedance-caused material-related phase change we want to obtain.

The effect of the container and liquid. To verify the impedance change is not only affected by the container but also the liquid inside, we carry out the following benchmark experiment. We first place the tag in the air, then attach it to an empty plastic container with a $4mm$ thickness and finally attach it to the container with 300ml sunflower oil (non-conductive liquid) inside. Other parameters including the tag-reader distance and the tag rotation are maintained the same. As demonstrated in Figure 4, the phase and RSS values for these three scenarios are quite different, which imply that the tag antenna's impedance is not only affected by the container, but also influenced by the liquid inside even the liquid is not touching the tag. So we can see that the antenna impedance can be affected even there is a spacing between the tag and the target. Our experiments show that as long as the spacing is not larger than 2cm, the target can still affect the tag's antenna impedance.

4 SYSTEM DESIGN

4.1 Material pattern construction

We propose to hop multiple channels to form a more unique material pattern to increase the material sensing accuracy. The tag antenna's impedance also changes with frequency [11] so that the *phase change* (material feature) caused by impedance change varies

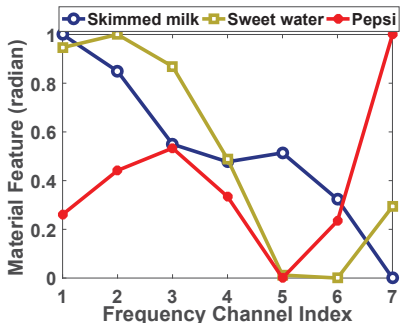

Figure 5: The designed material patterns for multiple targets.

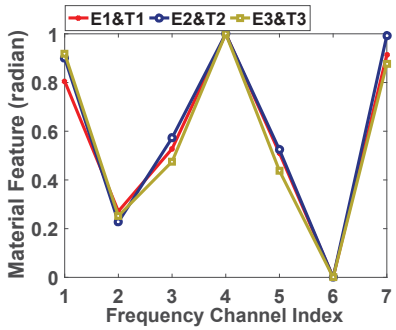

Figure 6: The material patterns for 0.231g/ml Saline water under different environments (E) and times (T).

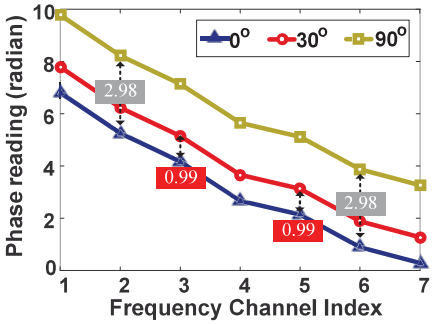

Figure 7: The impact of tag rotation on the phase readings across 7 random frequency channels.

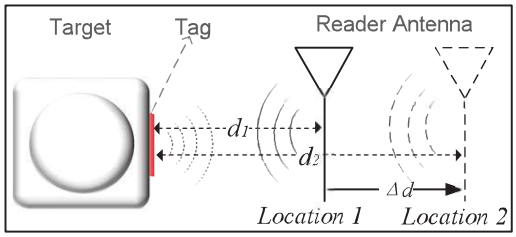

Figure 8: Removing the dependence of phase measurements on the tag-reader distance.

at different channels. We discover that this variation pattern across multiple frequency channels is *unique* and *stable* for each material. As shown in Figure 5, the material patterns for skimmed milk, sweet water and Pepsi are dramatically different which demonstrate the uniqueness of the material pattern. Moreover, the material patterns for 0.231g/mL saline water measured at three different environments and different timestamps are very similar to each other which demonstrate the stability of the material pattern, as shown in Figure 6. Hence, we employ the unique and stable feature-frequency pattern (material pattern[5]) for material sensing.

Number of channels employed for material sensing. Commodity RFID system has 50 frequency channels ranged from 902.75 to 927.25MHz [31, 45]. With a larger number of channels, we obtain a more unique feature-frequency pattern and accordingly higher identification accuracy. However, hopping to more channels takes time and leads to a larger latency. Impinj 420 RFID reader hops to one new channel every 200ms [31, 45]. It takes around 10s for a reader to hop across all 50 channels, which is a large latency. We find that, with just 7 channels, we are able to achieve good enough identification accuracy and the latency is significantly reduced to around 1.2s.

4.2 Dealing with distance-dependent phase

The random tag-reader distance introduces an unknown phase change to the phase reading (Eq. (6)), making extracting the material feature challenging. If we know the accurate distance between the tag and reader antenna, we can remove this phase change. However, this requires millimeter-level accuracy for distance estimation which is extremely difficult. We propose a novel method to address this problem. Specifically, we propose to remove the dependence on tag-reader distance with one more measurement at a random nearby location. To convey the rationale how Tagtag removes the unknown phase change caused by tag-reader distance, we consider a simple example shown in Figure 8.

The RSS reading which can be directly obtained from RFID reader has a relationship with the tag-reader distance as shown in Eq. (7). By moving the reader antenna to a random close-by location to obtain one more RSS reading, we have

$$RSS_i = 10\lg(G_t^2\Gamma_{tar}\frac{P_{Tx}}{1mW}T_rG_r^2(\frac{c}{4\pi f d_i})^4),\ i\in[1,2]. \quad (8)$$

Taking the difference of the two RSS readings, we have

$$40\lg(\frac{d_2}{d_1}) = RSS_1 - RSS_2. \quad (9)$$

We can see that even though the RSS reading is affected by target material as shown in Eq. (8), the RSS difference is only related to the two distances as shown in Eq. (9). Similarly, with the phase readings at two locations, we have

$$\phi_{B_i} = \Delta\phi_M + 2\pi(\frac{2d_i}{\lambda} - k_i) + \phi_0, k_i = \lfloor\frac{2d_i}{\lambda}\rfloor,\ i\in[1,2]. \quad (10)$$

We can obtain the following relationship

$$\frac{d_2}{d_1} = \frac{2\pi k_2 + \phi_{B_2} - \Delta\phi_M - \phi_0}{2\pi k_1 + \phi_{B_1} - \Delta\phi_M - \phi_0}. \quad (11)$$

With Eq. (9) and Eq. (11) both containing the same term $\frac{d_2}{d_1}$, we can cancel out $\frac{d_2}{d_1}$ and thus remove the two unknown distances d_1 and d_2 to derive the relationship below

$$\Delta\phi_M = \frac{2\pi(\Upsilon k_1 - k_2) + (\Upsilon\phi_{B_1} - \phi_{B_2})}{\Upsilon - 1} - \phi_0. \quad (12)$$

where $\Upsilon = 10^{\frac{RSS_1 - RSS_2}{40}}$. By now, we successfully remove the material feature's dependence on the distance d_1 and d_2. Note that k_1 and k_2 are integers in the range of [0, 12] if we consider a tag-reader distance of 2m.[6] There is only one pair of k_1 and k_2 that can make $\Delta\phi_M$ in the range of $[0, 2\pi]$ and we can easily search all possible pairs of k_1 and k_2. Moreover, since $k_1 = \lfloor\frac{2d_1}{\lambda}\rfloor$ and $k_2 = \lfloor\frac{2d_1+2\Delta d}{\lambda}\rfloor$, if the Δd is smaller than $\lambda/2$, we have $k_2 = k_1$ or $k_2 = k_1 + 1$. So if we restrict the distance Δd between two

[5]Note that the material pattern is normalized with method in [41].

[6]The wavelength of RFID signal is around 0.32m, thus the maximum value of k for a 2m distance is $\lfloor\frac{2*2m}{0.32m}\rfloor = 12$.

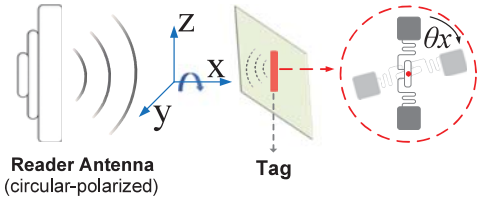

(a) Rotating a tag.

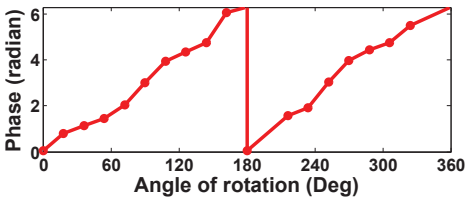

(b) Measured phase values for a rotating tag.

Figure 9: The phase shift brought by rotating a tag.

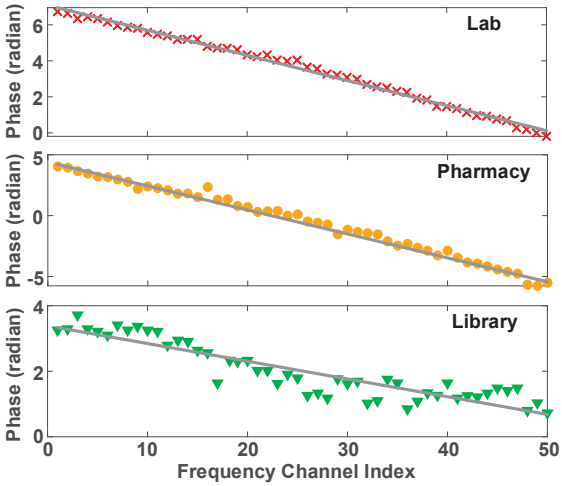

Figure 10: Phase measurements at different frequency channels roughly follow a liner relationship.

measurement locations to be smaller than $\lambda/2$, we can significantly decrease the computational complexity for searching from $O(N^2)$ to $O(N)$ where N is the number of possible integers for k_1 and k_2. Note that we do not need to know the exact value of Δd. So with a small random movement and one more measurement, we successfully remove the phase change dependence on tag-reader distance. Furthermore, with a small movement[7], we can still consider the multipath to be similar at two close-by locations.

4.3 Combating random tag rotation

A tag may be placed with a random rotation when attached to the target. To analyze the impact of tag rotation, we place a tag on a glass board and the tag-reader distance is set as 1.2m, as shown in Figure 9(a). Then we rotate the tag with the central point fixed without changing the tag-reader distance. Figure 9(b) plots the corresponding phase readings, where we can see the phase readings change roughly linearly with the rotation angle. Fortunately, the phase shift introduced by tag rotation is the same for all the channels. As shown in Figure 7, compared with the phase readings at the rotation 0°, other tag rotations (e.g., $30^\circ, 90^\circ$) introduce additional same phase shifts across all frequency channels. Thus, the overall material pattern is not changed but only moved up and down.

4.4 Impact of RSS errors and multipath

Note that besides the random rotation of the tag, the RSS's low resolution, RSS variations due to hardware noise, and multipath can all affect the material feature estimation.

RSS quantization error and RSS variation. The RSS readings from commodity RFID reader usually have a coarse resolution of 0.5dBm. Moreover, the hardware noise also cause variations in RSS readings. Although phase readings are employed for material identification, we do employ RSS readings to remove the distance dependence as described in Section 4.2.

We find that removing the effect of RSS errors is challenging. Thus, we do not try to eliminate them but keep them. Instead, we employ the information from multiple channels to form a unique pattern as shown in Figure 5 for material sensing and what we need to do is just to keep the RSS errors the same at multiple channels. Our method is explained as follows. Instead of measuring the RSS values which can vary differently at different channels, we only measure one RSS value at the first channel and calculate the rest RSS values by taking the RSS value measured at the first channel as a reference. By doing this, the RSS values calculated at other channels share the same errors as the first channel. Thus, although the RSS errors will cause the material feature to vary, the material feature across multiple channels vary in the same way. So the shape of the overall material pattern formed by multiple material features does not change but only moves up and down. To summarize, we employ the phase measurements at multiple channels but only one RSS measurement at the first channel to calculate the material pattern. By doing this, we make sure the rest material features on other channels contain exactly the same RSS quantization error and variation as the first channel. Thus, the impact of RSS error and variations are the same at all channels, which only moves the material pattern up and down but does not change the envelope (shape).

Multipath effect. To increase the communication range, most commodity RFID readers employ directional antenna. The Laird A9028R30NF antenna employed has a 70° elevation and azimuth beam widths. With directional antenna, the multipath issue is greatly alleviated. We further employ frequency hopping to pick "clean" channels with little multipath. We observe that, with frequency hopping, "clean" channels with little multipath can be found even in a rich multipath environment when directional antenna is employed. We obtain the phase values for all frequency channels in 3 different environments: Lab, Pharmacy and Library. If there is no multipath, the phase values measured at different channels exhibit a clear linear relationship with the frequency. As shown in Figure 10, even in the pharmacy and library with a lot of reflections, there exist more than 10 channels on which the phase values follow linear relationship with respect to the frequency channels. Note that frequency selective fading also exists and this linear phase-frequency relationship also helps us to pick the channels affected less by selective fading.

[7]We suggest a short distance of movement below 10cm.

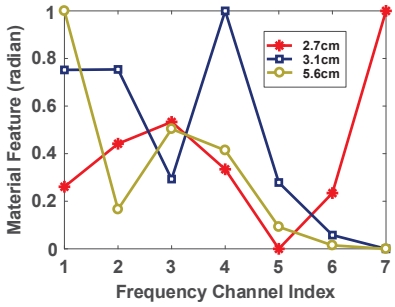

Figure 11: The material patterns for Pepsi under different liquid thicknesses.

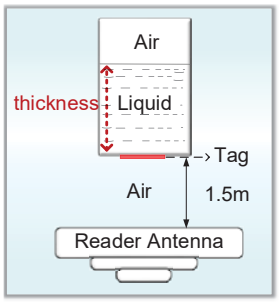

(a) Deployment.

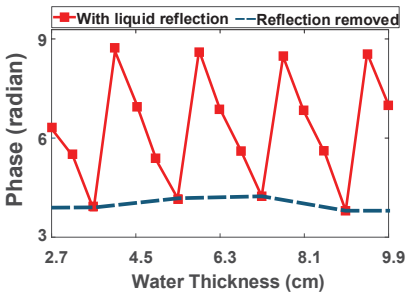

(b) Measured phase values vs. water thickness.

Figure 12: The phase variation caused by liquid reflection. Note that the operation range of Tagtag is about 3m. Here we set the tag-reader distance to 1.5m only for test.

4.5 Dealing with conductive liquid reflection

Different from non-conductive liquids, the conductive liquids reflect signals to the tag and different thicknesses cause different amounts of reflections. As a result, the reflection interferes the phase values received at the RFID reader and distorts the material pattern. As shown in Figure 11, Pepsi of different thicknesses have different amount of reflections and different material patterns.

4.5.1 Phase change due to liquid reflection.

Observation 1: *The phase change caused by conductive liquid reflection is determined by the thickness of the liquid as well as the material type.*

We conduct experiments to see the effect of liquid reflection. As shown in Figure 12(a), we put a tag at the bottom of a plastic container and pour different amounts of water with varying thickness h from 2.70cm to 9.90cm, at a step size of 0.45cm and we record the phase value for each thickness. As shown in Figure 12(b), the measured phase values vary with the water thickness periodically. To model the conductive liquid reflection, we refer to the theory of RF signal propagation [37]. When RF signal is transmitted from the air into a conductive liquid (such as water), reflected signal will be produced at the liquid surface. We quantify the reflected signal S_r with several variables

$$S_r = S_t \cdot \Gamma(\eta, \beta, L). \tag{13}$$

where S_t is the transmitted signal at the surface of the conductive liquid, Γ is the reflection coefficient, η denotes the liquid's intrinsic impedance ($\eta_{air} = 377\Omega$), $\beta = \frac{2\pi}{\lambda_{liquid}}$ stands for the signal's phase constant in the liquid, λ_{liquid} is the wavelength of the signal in the liquid, and L represents the liquid thickness. The reflection coefficient Γ [37] can be modeled as

$$\Gamma(\eta, \beta, L) = \frac{Z - \eta_{air}}{Z + \eta_{air}}. \tag{14}$$

$$Z = \eta \cdot \frac{\eta_{air} \cdot cos(\beta L) + j\eta \cdot sin(\beta L)}{\eta \cdot cos(\beta L) + j\eta_{air} \cdot sin(\beta L)}. \tag{15}$$

From Eq. (13), we know that the liquid reflection signal is related to both the liquid thickness (L) and liquid type (η, β).

4.5.2 Modeling the reflection.

Observation 2 *The phase values vary with the liquid thickness periodically and there is no liquid reflection when the thickness is* $\frac{n \cdot \lambda_{liquid}}{2}$ (n is a positive integer).

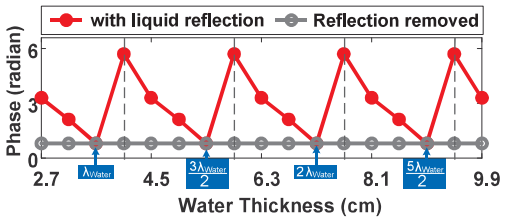

Figure 13: Theoretical phase values vs. water thickness.

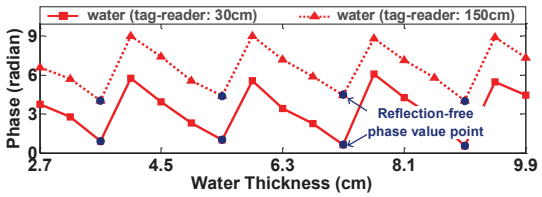

Figure 14: The phase-thickness relationships.

To understand the phase change brought in by signal propagation, we model the tag-reader communication when the tag is attached. The signal at RFID reader is a combination of direct reflection from the tag and reflection from the liquid. According to Eq. (14), the reflected signal from the liquid is related to the liquid's material type (β, η) and thickness L. We plug in the parameters for water [37] and plot the theoretical phase values for different liquid thicknesses in Figure 13. The results are consistent with the experimental measurements in Figure 12(b). The phase values change with a period of $0.5\lambda_{water}$ (half signal wavelength in water). More interestingly, when the water thickness is $0.5n \cdot \lambda_{water}$ (n is a positive integer), there is no reflection. The reason is given below. According to the reflection model in Section 4.5.1, if $L = \frac{n\lambda_{liquid}}{2}$, we have $sin(\beta L) = sin(\frac{2\pi}{\lambda_{liquid}} \cdot \frac{n\lambda_{liquid}}{2}) = 0$ and $cos(\beta L) = \pm 1$. Then according to Eq. (15), we obtain $Z = \eta_{air}$. At these particular thicknesses, water does not reflect any signal ($\Gamma = 0$).

4.5.3 Deriving reflection-free phase values.

To derive reflection-free phase value, we need to calculate the liquid thickness. We employ the phase change to estimate the liquid thickness. However, the unknown tag-reader distance also causes an unknown phase change at the reader. As shown in Figure 14, the phase readings vary with the liquid thickness. The tag-reader distance also changes the phase readings. Thus, with two unknown

Table 1: Test targets for material identification (ε_r: relative permittivity).

Water	Whole milk	Skimmed milk	Coke	Pepsi	Sprite	Sweet water	Red wine
ε_r: 76.7	Fat 0.04 g/ml ε_r : 72.93	Fat 0 g/ml ε_r : 70.43	Na 0.06 g/ml & Sugar 0.053 g/ml ε_r : 80.75	Na 0.12 g/ml & Sugar 0.112 g/ml ε_r : 83.65	Sugar 0.11 g/ml ε_r : 85.01	Sugar 0.276 g/ml ε_r : 69.31	Alcohol 12.5% vol ε_r: 40.6
Beer	**Liquor**	**Mineral water**	**Saline water**	**Vinegar**	**Edible oil**	**FanTa**	**Red Bull**
Alcohol 4.2% vol ε_r: 36.2	Alcohol 50% vol ε_r: 32.2	Mineral 49-116 g/ml ε_r: 78.24	Salt 0.183 g/ml ε_r: 87.35	Carbohydrate 4.9 g/ml ε_r: 72.35	Fat 100 g/ml ε_r: 15.3	Carbohydrate 0.106g/ml ε_r: 67.45	Caffeine 0.2mg/ml ε_r: 62.45
Wood	**Glass**	**Plastic**	**Ceramic tile**	**Rubber**	**Porcelain**	**Cardboard**	
Density 0.79 g/cm^3 ε_r: 4.1	SiO2 75.3% ε_r: 10.3	Density 1.68 g/cm^3 ε_r: 6.4	Water absorption rate $W_x > 10\%$ ε_r: 13.3	Hydrocarbon 94% ε_r: 5.7	Water absorption $W_x < 0.5\%$ ε_r:9.8	Wood pulp 100% ε_r: 2.75	

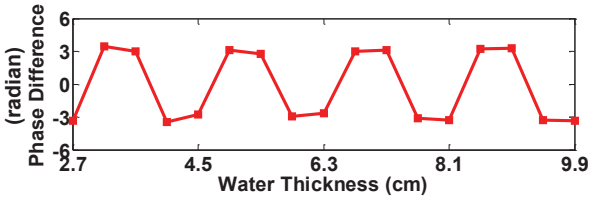

Figure 15: The relationship between phase difference of two overlapping tags and liquid thickness. ***This relationship does not change with different tag-reader distances.***

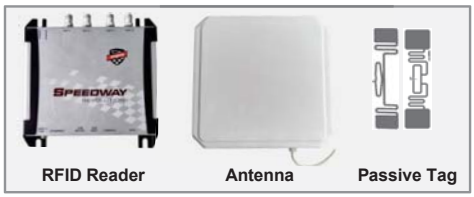

Figure 16: Hardware components.

Figure 17: Experiment environments.

variables and only one phase reading reported by the RFID reader, it is difficult to directly derive the liquid thickness. To address this problem, we remove the impact of tag-reader distance by employing two overlapping tags[8]. The distance-induced phase change is the same for the two tags. So if we subtract the phase readings from the two tags, we cancel out the distance-caused phase change and achieve a relationship between the phase and only liquid thickness in Figure 15. We can now use Figure 15 to calculate the liquid thickness L with the phase difference. With one phase difference value, multiple L can be obtained. We can employ any of them (L_r) for further processing. Now we can employ the thickness value L_r and the raw phase reading to obtain the reflection-free phase value. At a specific L_r, the difference between the measured phase value with and without liquid reflection is a constant ($\Delta\phi_r$) which can be measured beforehand. Thus, once the liquid thickness L_r is derived, the $\Delta\phi_r$ can be obtained and by subtracting $\Delta\phi_r$ from the raw phase readings, we successfully remove the effect of reflection and obtain the non-reflection phase values.

The reflection interference is determined by both the liquid thickness and liquid type (Section 4.4.1), thus deriving reflection-free phase values is challenging without knowing the exact material type. To address this problem, we test against all the liquid types stored in the database to find the best match. Specifically, for each liquid type in the database, we derive its reflection-free phase value and obtain the corresponding material pattern. We then calculate the DTW distance between the obtained material pattern and the stored material pattern in the database. We repeat the above process for all liquid types in the database and compute the corresponding DTW distances. The one generates the minimum DTW distance is determined as the material type.

[8]Note that the mutual coupling also affects each tag antenna's impedance. Thus, we consider the impedance after overlapping as the baseline, and measure the impedance change before/after both of them are attached to the target.

4.6 Material identification

We simply employ the DTW (Dynamic Time Warping) algorithm [41] to identify the material type by evaluating the similarity of the estimated material pattern with those material patterns in the database. The one generates the minimum DTW distance is determined as the target material. We employ an empirical threshold ρ to identify undefined new materials by comparing the resulted minimum DTW distance with ρ. If the minimum DTW distance is larger than ρ, it is identified as an undefined new material and stored in the database. Note that multi-class classification is employed in this work for material sensing.

5 IMPLEMENTATION

Frontend hardware. We implement a prototype of Tagtag using the commodity RFID Impinj R420 reader [45], which hops over 50 frequency channels within 902.75 $\sim$ 927.25MHz. Figure 16 presents the hardware components, including one reader, one directional circular-polarized antenna with a gain of 8dBi and two different passive tags (Impinj AZ-ET with a size of 1.4cm$\times$5.6cm and Aline AZ-9662 with a size of 1.7cm$\times$7cm). The reader is connected to a laptop via an Ethernet cable and continuously reports the phase and RSS readings. The reader together with the antenna is carried by

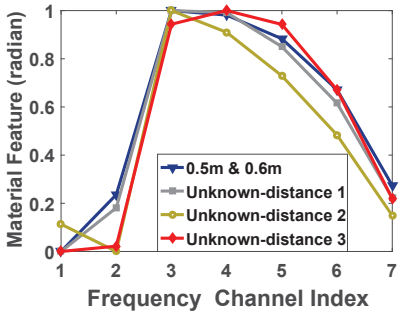

Figure 18: Material patterns for a wooden board under different tag-reader distances.

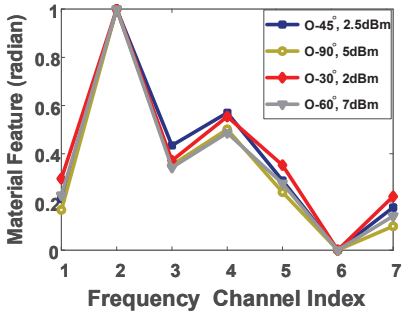

Figure 19: Material patterns under different tag rotations and RSS errors.

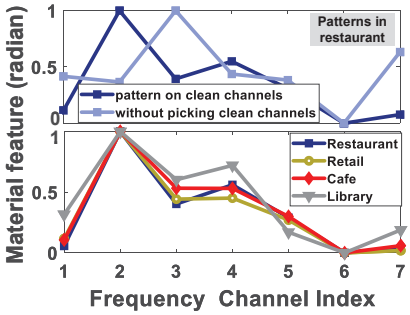

Figure 20: Material patterns under different environments.

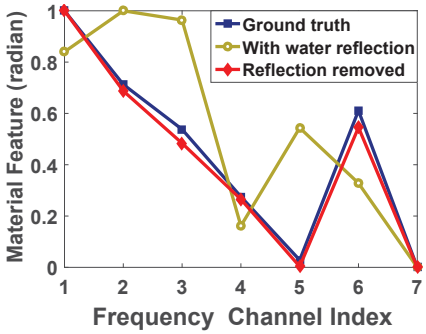

Figure 21: Material patterns with and without water reflection.

a robot to move to a second location for phase/RSS measurements to address the distance-dependence issue. In the experiments, the operation range of Tagtag is about 3m.

Note that, to identify the material type of non-conductive liquids, one tag is enough. For conductive liquids, two overlapping tags are needed to address the reflection problem. Thus, in Tagtag, we attach two overlapping RFID tags to the target (no matter it is a conductive material or not). The phase difference $\Delta\phi_r$ can be used to tell if there is liquid reflection. Specifically, when the phase difference is not equal to the phase difference in the air, there exists liquid reflection and we know the target material is conductive.

Backend implementation. We use C# and MATLAB for data collection and processing. The processing happens on a Lenovo Thinkpad laptop equipped with Intel(R) i5-5200U CPU and 8GB RAM. The software implementation is compatible with the Octane SDK Toolkit so that we can directly retrieve the phase and RSS readings from the RFID reader.

6 PERFORMANCE EVALUATION

In this section, we first present micro-benchmark experiments to verify the effectiveness of Tagtag. Then we evaluate the material identification performance of Tagtag with varying parameters. At the end, three case studies are presented to show the real-life applications of our system.

Test targets. We employ 23 different types of materials (Table 1) including 16 commonly seen liquids and 7 solid objects (non-conductive material) to evaluate the performance of Tagtag. Among the liquids, the sunflower oil is non-conductive and the rest are conductive. For the liquids, each of them is poured into an identical cylindrical plastic container (height: 26cm; diameter: 16.4cm) for testing. The solids for testing are different in size.

Data Collection: Before identifying the material types, Tagtag first obtains the material patterns for all the test targets and stores them in database. For each conductive liquid, we also collect the phase values for varying thicknesses at a step size of 0.1cm within a half wavelength of the signal in the liquid. Note that both the liquid and the container affect the tag antenna impedance. To remove the impact of container, Tagtag collects a set of measurements as the baseline data when the container is empty. The baseline data is then used to remove the effect of container and only needs to be measured once.

Experimental environments: We conduct experiments to evaluate the performance of Tagtag in four indoor environments: a restaurant, a cafe, a retail store and a library. Figure 17 presents a snapshot of these environments corresponding to different multipath conditions. The sensing range of Tagtag is up to 3m.

6.1 Micro benchmarks

We start with three benchmark experiments to validate the effectiveness of our proposed methods.

Removing the unknown tag-reader distance. To evaluate whether our method of removing the unknown tag-reader distance caused phase is effective, we calculate the material patterns for a beech wood with a size of 10cm×10cm×3cm under different tag-reader distances. We first construct the material pattern with measurements at two known locations with tag-reader distances of 0.5m and 0.6m, respectively. Then we randomly move the reader antenna three times and calculate the material patterns without knowing the tag-reader distances. For the three material patterns without knowing the distances, we employ the method in Section 4.2 to remove the unknown distances. Figure 18 presents these material patterns and we can see that the material patterns without knowing the tag-reader distances are very similar to the one obtained by knowing the tag-reader distances.

Addressing the effect of tag rotation, RSS errors and multipath. The random tag rotation, RSS errors and multipath can decrease the material identification accuracy. We first consider four groups of parameters with different tag rotations and RSS errors. Figure 19 presents the material patterns for a piece of ceramic tile

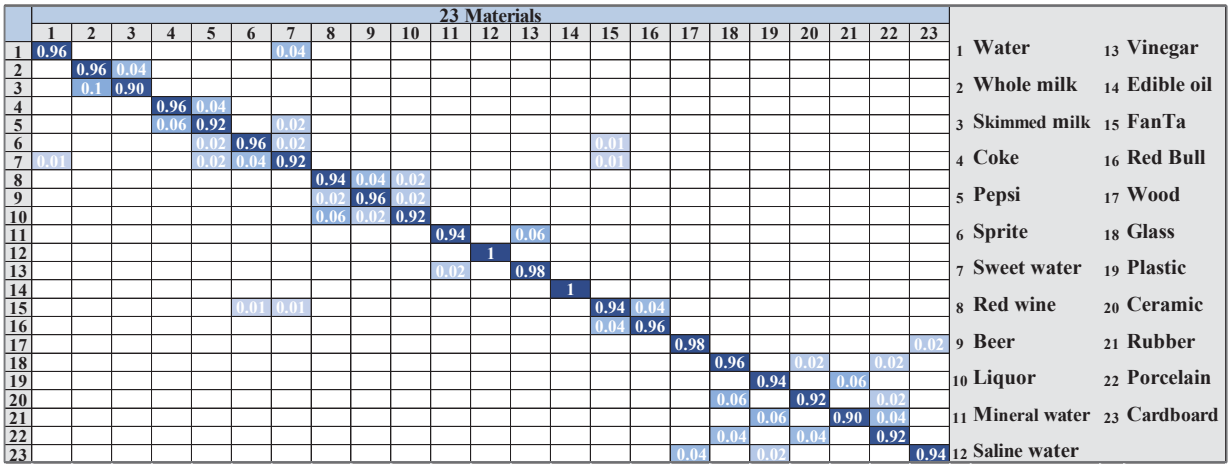

Figure 22: Identification accuracies for 23 materials (16 liquids and 7 solids).

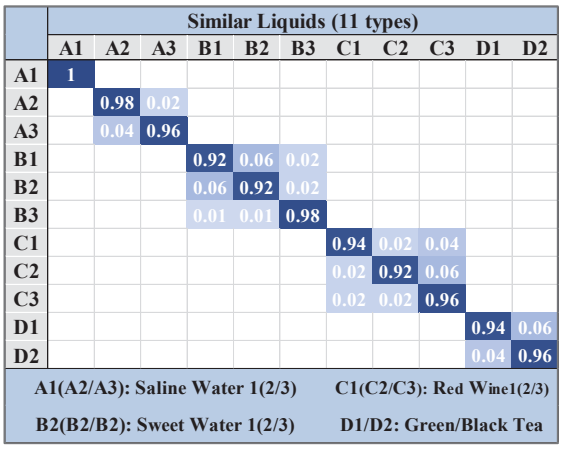

Figure 23: Identification accuracies for similar liquids.

(12cm×12cm×3cm) with four groups of parameters. The parameters are tag rotations and RSS errors, i.e., (45°, 2.5dBm), (90°, 5dBm), (30°, 2dBm) and (60°, 7dBm). We can see that the patterns are very similar to each other, demonstrating we effectively remove the impact of those parameters. To further show the effectiveness of addressing multipath effect, we present the material patterns with and without picking clean channels in Figure 20 (up). We can see that the material patterns can be quite different. We further show the material patterns with picking clean channels under four different experimental environments, i.e., restaurant, retail, cafe and library in Figure 20 (below). The patterns are stable and similar. These results demonstrate the effectiveness of picking clean channels in addressing multipath.

Addressing liquid reflection. Two overlapping tags are put at the bottom of a cylindrical plastic container (height: 26cm, diameter: 16.4cm). We first collect the phase/RSS measurements with a water thickness of 3.6cm at which the reflection is 0. The corresponding material pattern is obtained as the ground truth. We next collect measurements for water with a thickness of 4cm where there exists reflection and the corresponding material pattern with reflection is obtained. We then apply the method proposed in this work to remove the effect of reflection and generate the proposed material pattern with reflection removed. Figure 21 shows that with the proposed reflection-removal method, the processed material pattern matches the ground truth very well. This demonstrates the effectiveness of our method in addressing the liquid reflection interference.

6.2 Material identification performance

Overall Performance. We employ 23 different materials listed in Table 1 to evaluate the material identification accuracy of Tagtag. For each material, we run the experiments 50 times with 10 objects of the same material. For each object, we carry out experiments 5 times with different tag-reader distances. We pour the liquids into a cylindrical plastic container and attach one pair of overlapping tags on the lateral side of the container. As shown in Figure 22, the average identification accuracy for 7 solids is 93.7% while for the 16 liquids, Tagtag achieves an average accuracy of 95.1%. Specifically, the identification accuracies of solids at the four experiment environments shown in Figure 17, i.e., restaurant, cafe, library and retail store, are 96.6%, 95.7%, 90.6% and 92.0%, respectively. The corresponding accuracies for liquids are 97.4%, 96.0%, 93.3% and 93.9%, respectively. For similar materials i.e., Pepsi, Coke, whole milk and skimmed milk, the achieved average accuracy is still higher than 94%.

Similar liquids. Additional experiments are conducted to check whether Tagtag is able to differentiate the same type of liquids with slightly different concentrations, e.g., saline water (0.072g/ml, 0.116g/ml and 0.231g/ml), sweet water (0.087g/ml, 0.187g/ml and 0.276g/100ml), red wine (alcohol: 8.5%, 11.5%, 15%) and tea (green/black tea). As shown in Figure 23, we are still able to achieve an average accuracy of 95.3%.

6.3 Performance with varying parameters

In this section, we vary the parameters to test the robustness of our system.

Impact of reader's direction with respect to the tag. We first run experiments to evaluate how the reader's direction with respect to the tag affects the performance. We place the tags on the lateral side of a cylindrical plastic container (height: 26cm, diameter: 16.8cm) which contains each liquid listed in Table 1 with a volume of 3000ml.

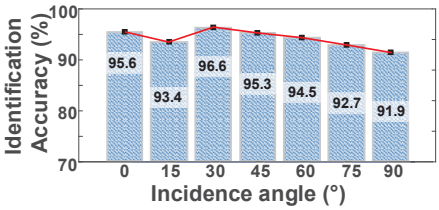

Figure 24: Impact of reader's direction with respect to the tag.

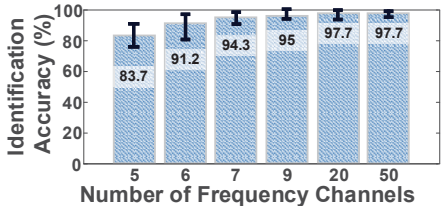

Figure 25: Impact of frequency channels.

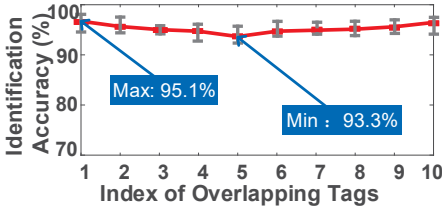

Figure 26: Impact of using different tags.

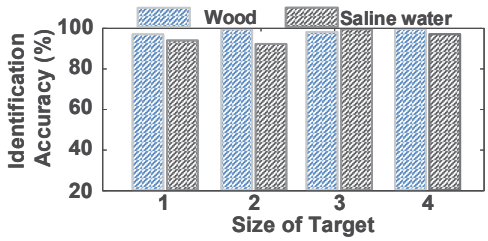

Figure 27: Impact of target size.

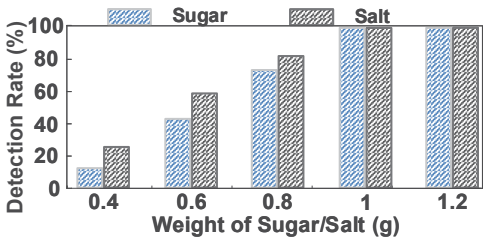

Figure 28: Tagtag's sensibility on detecting whether the 100ml pure water is mixed with other materials.

We define the direction perpendicular to the tag surface as 0°. We vary the reader's direction with respect to the tag from 0° to 90° at a step of 15°. For each direction, we repeat the experiments 30 times with different tag-reader distances. Figure 24 plots the corresponding identification accuracies. A slightly lower accuracy at 90° may be caused by lower SNR (signal-noise ratio) as the tag antenna gain is slightly lower at this direction. From the results presented, we can see that the identification accuracies are not affected much by the reader's direction. This result demonstrates the high flexibility of Tagtag and the reader can be placed at a large range of directions.

Impact of number of frequency channels. In general, with more channels, Tagtag is able to achieve a higher material identification accuracy as shown in Figure 25. We conduct experiments using 23 test targets (16 liquids and 7 solids). The identification accuracy is 83.7% for five channels, 94.3% for seven channels, and 97.7% for twenty channels. With more channels, the frequency-feature pattern is more unique and thus can present better performance. We also observe that with more than 20 channels, the improvement gets saturated and does not change much. Since more frequency channels mean larger latency, we employ 7 channels to maintain a good balance between latency and accuracy. With 7 channels, the latency is around 1.2s while the accuracy is very close to that with 50 channels.

Impact of tag diversity. To evaluate the impact of tag diversity, we employ 10 Impinj AZ-ET tags and 10 Aline AZ-9662 tags to form 10 pairs of overlapping tags. Then we use each pair to evaluate the performance of Tagtag, and measure the corresponding identification accuracies for 23 test targets. As shown in Figure 26, the accuracies fluctuate in a relatively small range of 3%. We also observe that the identification accuracy can be reduced if the sizes of the overlapping tags are very different so we suggest to use two similar size tags.

Impact of target size. We vary the target size to see the impact on the identification accuracy. We test one solid target (beech wood) and one conductive liquid (0.183g/ml saline water). We repeat the experiments 50 times. For the solid targets, the thickness is the same (3cm) and four different side dimensions, *i.e.*, 30×42cm, 20×30cm, 15×20cm and 10×10cm are tested. For the liquid experiment, we pour the saline water into four cylindrical plastic containers of different diameters and heights, *i.e.*, (10.5cm, 12.6cm), (11.6cm, 14.7cm), (13.4cm, 20.5cm) and (16.4cm, 26cm). As shown in Figure 27, the identification accuracies for the wood and saline water with varying sizes are always higher than 95%, demonstrating Tagtag's robustness against target sizes.

6.4 Case Study

In this section, we apply Tagtag in three case studies: (i) we apply Tagtag to detect whether the target water is pure water; (ii) anti-fake detection: we apply Tagtag to check whether a small amount of water added in the liquor (50% alcohol) can be detected; we also apply Tagtag to see if we can identify two bottles of fake luxury CHANEL perfume and (iii) whether Tagtag is able to differentiate fresh milk from expired milk exposed in the air for a few hours.

Case I: pure water detection. To detect whether the target pure water is mixed with other materials, we put a small amount of salt or sugar (e.g., 0.2g, 0.8g and 1g, etc.) separately into 100ml pure water, and then calculate the corresponding DTW distance between the pure water's material pattern and the mixture's pattern. If the DTW distance is larger than the empirical threshold ξ_{water}, Tagtag detects there is something added in the water. We measure the pure water's material pattern for 50 times and determine the value of ξ_{water} as the maximum DTW distance between two pure water's material patterns. By choosing the maximum DTW distance as the threshold, we guarantee the false positive rate (FPR) is extremely small. For each weight of salt/sugar, we repeat the experiments 30 times and calculate the corresponding detection rate. Figure 28 shows that as long as more than 1g salt/sugar is added into 100ml water, we can 100% detect the water is not pure water anymore.

Case II: anti-fake detection. In this case study, we use perfume and liquor to examine Tagtag's anti-fake capability. For liquor experiment, we would like to study how much water needs to be added into the liquor until a difference can be detected. In real life, we can easily attach cheap RFID tags to the bottle for this purpose. We conduct experiments with 6 different amounts of water added into the 500ml liquor with an alcohol concentration of 50%, from 2ml to

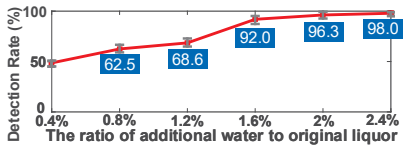

(a) The detection rate for liquor experiment.

(b) CHANEL perfume (EAU DE TOILETTE).

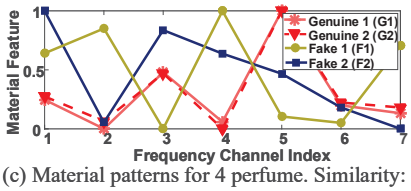

(c) Material patterns for 4 perfume. Similarity: G1&G2: 99%, G1& F1:72%, G1&F2: 56%.

Figure 29: The results for anti-fake detection (Case Study II).

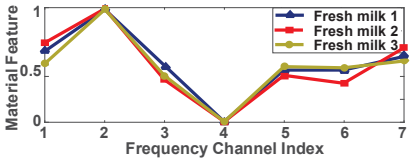

(a) Material patterns for 3 fresh milk.

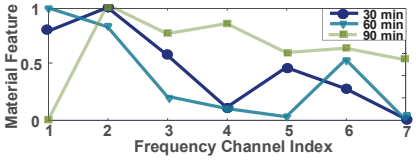

(b) Material patterns for different exposure times.

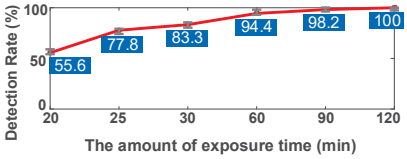

(c) Detection rate for expiration (bottle opened).

Figure 30: The results for milk expiration detection (Case Study III).

12ml at a step size of 2ml. We repeat the experiments 30 times for each amount of water. We choose the empirical threshold ξ_{liquor} in the same way as the previous case study. As shown in Figure 29(a), the detection rate is higher than 96% when 2% water is added.

For perfume identification, four bottles of 100ml CHANEL perfume are employed as shown in Figure 29(b) with two genuine and two different fake ones. While their colors are very the same, we employ Tagtag to see if we can detect a clear difference between the genuine and fake ones. As shown in Figure 29(c), the material patterns for the two bottles of genuine perfume are very close and they are dramatically different from the two fake ones. The similarity index[9] between "Genuine 1" and "Genuine 2", "Fake 1", "Fake 2" are 99%, 72% and 56% respectively.

Case III: detecting the expiration of milk. To identify whether the milk is fresh or not, we expose 1000ml fresh milk in the air at a temperature of $85^\circ F$ and monitor its material pattern change with different amounts of exposure time. We repeat the experiments 30 times for each exposure time. The threshold ξ_{milk} is chosen in the same way as the previous study. As shown in Figure 30(a), we measure three bottles of fresh milk (1000ml) at the same time and the corresponding material patterns are very similar. Further, Figure 30(b) demonstrates that the pattern is changed and can be detected after 30min exposure in the air at $85^\circ F$. As shown in Figure 30(c), after 90min, we can detect non-fresh milk at a detection rate higher than 98.2%.

7 DISCUSSION

The range of tag-reader distance. The tagging on a target can cause a decrease in the communication range of the tag and reader. The proposed system does not work with metal container because the tag can hardly be read when attached to a metal surface. There are dedicated tags designed for metal surface which we plan to give a try in our future work.

Random frequency hopping. For security reasons, the RFID reader does not hop to channels sequentially. We observe that the hopping sequence does not change as long as the hardware is not power restarted. When we employ 7 channels for material identification, we make sure we employ the same 7 channels.

[9]We employ a modified version of DTW [41] to calculate the similarity index.

Differentiating materials with similar material pattern. Limited by the resolution of phase readings retrieved from the commodity RFID reader, it is still challenging for Tagtag to differentiate materials with very similar material pattern. For example, Tagtag can differentiate pure water from 10mg/ml saline water. However, when the concentration is decreased to 2mg/ml, Tagtag cannot detect it because the material pattern of the 2mg/ml saline water is so close to pure water. Furthermore, we want to point out that Tagtag is still not able to sense mixed materials.

Fake material construction. Tagtag presents one interesting way of detecting fake materials. On the other hand, constructing fake material that cannot be detected by Tagtag is one direction we would like to explore in the future. Specifically, by carefully tuning the component to make the fake material exhibit very similar material pattern as the genuine material, it then can not be detected by Tagtag. Constructing fake material that can fool multiple systems (e.g., both Tagtag and TagScan [42]) can be even more challenging.

8 CONCLUSION

In this paper, we demonstrate the possibility of attaching cheap RFID tags to a target for highly accurate material sensing. By employing the high-resolution phase change caused by the tag antenna's impedance change when attached to a target, Tagtag is able to differentiate even very similar materials such as Pepsi and Coke. We successfully address multiple issues including the random distance, random tag rotation, RSS errors, multipath and conductive liquid reflection interference, making Tagtag a promising candidate for real-life deployment.

9 ACKNOWLEDGEMENTS

This work was partially supported by the National Natural Science Foundation of China (NSFC) under Grant Numbers 61572402, 61602382 and 61672428, the Science and Technology Innovation Team Support Project of Shaanxi under Grant 2018TD-026, and the International Science and Technology Cooperation Project under Grant 2019KWZ-05.

REFERENCES

[1] N. Adair. Radio frequency identification (rfid) power budgets for packaging applications. *PGK*, 2005.

[2] E. M. Amin, R. Bhattacharyya, S. Kumar, and S. Sarma. Towards low-cost resolution optimized passive uhf rfid light sensing. In *WAMICON*, pages 1–6, 2014.

[3] C. Balas, G. Epitropou, A. Tsapras, and N. Hadjinicolaou. A novel hyperspectral camera and analysis platform for the non-destructive material identification and mapping: An application in paintings by el greco. In *IST*, pages 211–215. IEEE, 2016.

[4] R. Bhattacharyya, C. Floerkemeier, and S. Sarma. Low-cost, ubiquitous rfid-tag-antenna-based sensing. *IEEE*, 98(9):1593–1600, 2010.

[5] R. Bhattacharyya, C. Floerkemeier, and S. Sarma. Rfid tag antenna based sensing: Does your beverage glass need a refill? In *RFID*, pages 126–133, 2010.

[6] R. Bhattacharyya, C. Floerkemeier, S. Sarma, and D. Deavours. Rfid tag antenna based temperature sensing in the frequency domain. In *RFID*, pages 70–77. IEEE, 2011.

[7] L.-X. Chuo, Z. Luo, D. Sylvester, D. Blaauw, and H.-S. Kim. Rf-echo: A non-line-of-sight indoor localization system using a low-power active rf reflector asic tag. In *MobiCom*, pages 222–234. ACM, 2017.

[8] A. Dhekne, M. Gowda, Y. Zhao, H. Hassanieh, and R. Roy Choudhury. Liquid: A wireless liquid identifier. In *MobiSys*, pages 1–13, 2018.

[9] D. M. Dobkin. *The RF in RFID: passive UHF RFID in practice*. Newnes, 2012.

[10] D. M. Dobkin and S. M. Weigand. Environmental effects on rfid tag antennas. In *MTTS*, pages 135–138, 2005.

[11] K. Fujimoto. *Mobile antenna systems handbook*. Artech House, 2008.

[12] H. Fukuda, K. Kosaka, and W. Hattori. Rfid-based sensing technology with microstrip lines. In *Sensors*, pages 839–842, 2014.

[13] C. Gao and Y. Li. Livetag: Sensing human-object interaction through passive chipless wifi tags. In *NSDI*, pages 165–178, 2018.

[14] J. D. Griffin, G. D. Durgin, A. Haldi, and B. Kippelen. Radio link budgets for 915 mhz rfid antennas placed on various objects. In *Texas Wireless Symposium*, 2005.

[15] U. Ha, Y. Ma, Z. Zhong, T. Hsu, and F. Adib. Learning food quality and safety from wireless stickers. In *Hotnets*, pages 106–112. ACM, 2018.

[16] P. Hillyard, C. Qi, A. Al-Husseiny, G. D. Durgin, and N. Patwari. Focusing through walls: An e-shaped patch antenna improves whole-home radio tomography. In *RFID*, pages 174–181. IEEE, 2017.

[17] E. Jones, S. D. Pringle, and Z. Takats. Ambient ionization mass spectrometry imaging platform for direct mapping from bulk tissue, 2 2018. US Patent App. 15/555,818.

[18] K. Joshi, D. Bharadia, M. Kotaru, and S. Katti. Wideo: fine-grained device-free motion tracing using rf backscatter. In *NSDI*, pages 189–204, 2015.

[19] M. A. A. H. Khan, R. Kukkapalli, P. Waradpande, S. Kulandaivel, N. Banerjee, N. Roy, and R. Robucci. Ram: Radar-based activity monitor. In *INFOCOM*, pages 1–9. IEEE, 2016.

[20] B. Korany, C. R. Karanam, and Y. Mostofi. Adaptive near-field imaging with robotic arrays.

[21] M. Kotaru, P. Zhang, and S. Katti. Localizing low-power backscatter tags using commodity wifi. In *CoNEXT*, pages 251–262. ACM, 2017.

[22] S. Kumar and D. Katabi. Decimeter-level localization with a single wifi access point. In *NSDI*, pages 165–178, 2016.

[23] T. Li, Q. Liu, and X. Zhou. Practical human sensing in the light. In *MobiSys*, pages 71–84, 2016.

[24] Y. Ma, N. Selby, and F. Adib. Minding the billions: Ultra-wideband localization for deployed rfid tags. In *MobiCom*, pages 248–260. ACM, 2017.

[25] S. Manzari, C. Occhiuzzi, S. Nawale, A. Catini, C. D. Natale, and G. Marrocco. Humidity sensing by polymer-loaded uhf rfid antennas. *Sensors*, 12(9):2851–2858, 2012.

[26] W. Mao, J. He, and L. Qiu. Cat: high-precision acoustic motion tracking. In *MobiCom*, pages 69–81. ACM, 2016.

[27] W. Mao, Z. Zhang, L. Qiu, J. He, Y. Cui, and S. Yun. Indoor follow me drone. In *MobiSys*, pages 345–358. ACM, 2017.

[28] P. Melgarejo, X. Zhang, P. Ramanathan, and D. Chu. Leveraging directional antenna capabilities for fine-grained gesture recognition. In *UbiComp*, pages 541–551. ACM, 2014.

[29] R. Nandakumar, B. Kellogg, and S. Gollakota. Wi-fi gesture recognition on existing devices. *arXiv preprint arXiv:1411.5394*, 2014.

[30] K. Ogawa, T. Hirokawa, and S. Nakamura. Identification of a material with a photon counting x-ray ct system. In *Nuclear Science Symposium Conference Record*, pages 2582 – 2586, 2011.

[31] S. Pradhan, E. Chai, K. Sundaresan, L. Qiu, M. A. Khojastepour, and S. Rangarajan. Rio: A pervasive rfid-based touch gesture interface. In *MobiSys*, pages 261–274. ACM, 2017.

[32] J. T. Prothro, G. D. Durgin, and J. D. Griffin. The effects of a metal ground plane on rfid tag antennas. In *Antennas and Propagation Society International Symposium*, pages 3241–3244. IEEE, 2006.

[33] B. M. Rankin, J. Meola, D. L. Perry, and J. R. Kaufman. Methods and challenges for target detection and material identification for longwave infrared hyperspectral imagery. In *SPIE Defense Security*, pages 1–12, 2016.

[34] W. F. Schmidt and K. Yoshino. Ion mobilities in non-polar dielectric liquids: silicone oils. *IEEE Transactions on Dielectrics & Electrical Insulation*, 22(5):2424–2427, 2015.

[35] L. Shangguan, Z. Zhou, and K. Jamieson. Enabling gesture-based interactions with objects. In *MobiSys*, pages 239–251. ACM, 2017.

[36] C. Shi, J. Liu, H. Liu, and Y. Chen. Smart user authentication through actuation of daily activities leveraging wifi-enabled iot. In *Mobihoc*, page 5. ACM, 2017.

[37] J. R. Wait. *Electromagnetic Wave Theory*. Higher Education Press, 2002.

[38] G. Wang, C. Qian, J. Han, W. Xi, H. Ding, Z. Jiang, and J. Zhao. Verifiable smart packaging with passive rfid. In *UbiComp*, pages 156–166. ACM, 2016.

[39] J. Wang, O. Abari, and S. Keshav. Challenge: Rfid hacking for fun and profit. *sensors*, 3(14):15, 2018.

[40] J. Wang, H. Jiang, J. Xiong, K. Jamieson, X. Chen, D. Fang, and B. Xie. Lifs: low human-effort, device-free localization with fine-grained subcarrier information. In *MobiCom*, pages 243–256. ACM, 2016.

[41] J. Wang and D. Katabi. Dude, where's my card?: Rfid positioning that works with multipath and non-line of sight. *SIGCOMM*, 43(4):51–62, 2013.

[42] J. Wang, J. Xiong, X. Chen, H. Jiang, R. K. Balan, and D. Fang. Tagscan: Simultaneous target imaging and material identification with commodity rfid devices. In *MobiCom*. ACM, 2017.

[43] B. H. Waters, A. P. Sample, and J. R. Smith. Adaptive impedance matching for magnetically coupled resonators based on passive uhf rfid. In *PIERS Proceedings*, pages 694–701. Citeseer, 2012.

[44] T. Wei and X. Zhang. mtrack: High-precision passive tracking using millimeter wave radios. In *MobiCom*, pages 117–129. ACM, 2015.

[45] T. Wei and X. Zhang. Gyro in the air: tracking 3d orientation of batteryless internet-of-things. In *MobiCom*, pages 55–68. ACM, 2016.

[46] J. Xiong, K. Sundaresan, and K. Jamieson. Tonetrack: Leveraging frequency-agile radios for time-based indoor wireless localization. In *MobiCom*, pages 537–549. ACM, 2015.

[47] L. Yang, Y. Chen, X.-Y. Li, C. Xiao, M. Li, and Y. Liu. Tagoram: Real-time tracking of mobile rfid tags to high precision using cots devices. In *MobiCom*, pages 237–248. ACM, 2014.

[48] L. Yang, Y. Li, Q. Lin, X. Y. Li, and Y. Liu. Making sense of mechanical vibration period with sub-millisecond accuracy using backscatter signals. In *MobiCom*, pages 16–28. ACM, 2016.

[49] H.-S. Yeo, G. Flamich, P. Schrempf, D. Harris-Birtill, and A. Quigley. Radarcat: Radar categorization for input & interaction. In *UIST*, pages 833–841. ACM, 2016.

[50] S. Yun, Y.-C. Chen, H. Zheng, L. Qiu, and W. Mao. Strata: Fine-grained acoustic-based device-free tracking. In *MobiSys*, pages 15–28. ACM, 2017.

[51] C. Zhang and X. Zhang. Pulsar: Towards ubiquitous visible light localization. In *MobiCom*, pages 33–35. ACM, 2017.

[52] O. Zhang and K. Srinivasan. Mudra: User-friendly fine-grained gesture recognition using wifi signals. In *CoNEXT*, pages 83–96. ACM, 2016.

[53] Z. Zhao, J. Wang, X. Zhao, C. Peng, Q. Guo, and B. Wu. Navilight: Indoor localization and navigation under arbitrary lights. In *INFOCOM*, pages 1–9. IEEE, 2017.

[54] Y. Zhu, Y. Zhu, B. Y. Zhao, and H. Zheng. Reusing 60ghz radios for mobile radar imaging. In *MobiCom*, pages 103–116. ACM, 2015.